Inhomogeneous states in a small magnetic disk with single-ion surface anisotropy

V. E. Kireev* and B. A. Ivanov†
Institute of Magnetism NAS of Ukraine, 36-B Vernadskii avenue, 03142 Kiev, Ukraine
(Received 13 November 2002; revised manuscript received 3 June 2003; published 24 September 2003)

We investigate analytically and numerically the ground and metastable states for easy-plane Heisenberg magnets with single-ion surface anisotropy and disk geometry. The configurations with two half vortices at the opposite points of the border are shown to be preferable for strong anisotropy. We propose a simple analytical description of the spin configurations for all values of surface anisotropy. The effects of lattice pinning lead to appearance of a set of metastable configurations.

DOI: 10.1103/PhysRevB.68.104428 PACS number(s): 75.70.Rf, 75.25.+z

The progress of nanotechnology permits creation of ensembles of fine magnetic particles (magnetic dots) of nanometer scale, see for review Ref. 1. Magnetic dots in the form of cylinders or prisms have been made of soft magnetic materials such as Co and permalloy[2–6] or highly anisotropic materials such as Dy and FePt, see Refs. 7,8. Magnetic dots and their arrays are of interest both in the basic and applied magnetism with potential applications including high-density magnetic storage media.[9]

Usually a small magnetic particle is considered as being in the monodomain state with a homogeneous saturated magnetization (or Néel vector for antiferromagnets). During the past few years it has been established that the distribution of magnetization within the dots made of soft magnetic materials can be quite nontrivial; namely, various inhomogeneous states resulting from the magnetic dipole-dipole interaction appear. In recent years interest in such states for submicron particles has risen significantly. A small enough nonellipsoidal dot exhibits a single-domain, nearly uniform magnetization state, so-called *flower* and *leaf* states.[6,10–12] When increasing the size of the dot above a critical value, vortex state occurs.[3,13–17] The main property of such states is the nonsaturating value of the total dot magnetization, nearly zero for vortex states and nearly saturated, but less than saturated, for leaf and flower states.

O'Shea and co-workers[18–20] have observed nonsaturated states for the rare-earth ferromagnetic granules with high anisotropy and the size about of 5 nm. A possible explanation of this fact is that these particles are in nonuniform states.[39] On the other hand, it is clear that the concepts of nonuniform states referred to above and caused by a magnetic dipole interaction cannot be applied directly to such small particles made with highly anisotropic material. In this regard, some other sources of nonuniformity need to be found.

The appearance of nonuniform states for small bcc atomic clusters by taking into account the *single-ion* surface anisotropy have been shown numerically by Dimitrov and Wysin.[21,22] Garanin and Kachkachi in the recent work[23] investigated the effective anisotropy caused by such a nonuniform spin distribution for small magnetic particles. The difference of the properties of the spins on the surface and in bulk could be considered as a defect destroying the homogeneity of a sample. It is clear that due to the surface a homogeneous ordering is distorted or even broken.

In real magnets the surface could produce the surface anisotropy for two reasons. First, the main origin of magnetic anisotropy can be caused by the anisotropy of spin-spin interactions (the case of *exchange* anisotropy). For this case even on an ideal atomically smooth surface the spins have different coordination numbers than in bulk, and consequently the intensity of the exchange interaction changes. For the surface exchange anisotropy the direction of the chosen axis is the same as in bulk and has no connection to the surface. This effect could lead to the nonuniform states in some special cases only, mostly in the presence of an external magnetic field, for example, the surface spin-flop transition,[24,25] and the states caused by the magnetic field for easy-axial ferromagnets.[26] Second, in real magnets surface atoms have a different environmental symmetry. Thus, the surface distorts a crystalline field that acts on a magnetic ion, and the anisotropy is changed drastically. It leads to a specific *single-ion* surface anisotropy for the spins with a preferred axis coinciding with the normal to the surface. This model is considered by Dimitrov and Wysin for fcc iron clusters;[21,22] we would like to investigate this case both analytically and numerically. Note that the surface effects, in particular, the surface anisotropy, have been considered by many authors,[27,28] but in most of these works the ground states have been assumed to be homogeneous, and the surface terms are only accounted in dynamics. On the other hand, it is obvious that for fine magnetic particles the role of the surface becomes much more important than for bulk materials. The effects caused by the surface considered as a defect are proportional to $N^{-1/3}$, and their role increases when the size of the particle tends to the nanometer scales.

Note that similar problems arise in the other domains of condensed-matter physics, where the role of surface is important. These are textures in liquid crystals[29] and in a superfluid ^{3}He, see Ref. 30. For the A phase of ^{3}He (^{3}He-A) the unit-vector order parameter $\boldsymbol{l}$, $\boldsymbol{l}^2=1$ is perpendicular to the surface of a vessel. ^{3}He cannot be in equilibrium with its own vapor; it fills the vessel completely at temperatures when it is superfluid ($T\lesssim 2$ mK). Thus, the vector $\boldsymbol{l}$ should be perpendicular to the surface of the ^{3}He-A sample. The analysis shows that the order parameter becomes nonuniform, and, moreover, it is singular for any simply connected vessel.[30]

It is clear that such effects may be observed in all finite samples of ordered media with vector order parameter and a strong surface anisotropy of the form $B(\boldsymbol{m}\cdot\boldsymbol{n})^2$, where $\boldsymbol{n}$ is the normal to the surface, $\boldsymbol{m}$ is the order parameter, and B is the constant of single-ion surface anisotropy, which orients $\boldsymbol{m}$ with respect to the surface. For the ^{3}He-A, the boundary condition could be described as a limit of an *infinitely strong* surface anisotropy $B<0$, $|B|\to\infty$, with easy axis perpendicular to the surface. The concept developed for ^{3}He-A could be a good guide for a theory of fine magnetic particles with surface anisotropy. On the other hand, the situation for magnets is more general: the magnitude of the surface anisotropy for magnets is finite, and the magnetic moment could be inclined with respect to the axis of surface anisotropy. As we will show below, finiteness of anisotropy could lead to the states with nonuniform spin distributions but without singularities.

The outline of the paper is as follows. In Sec. I we discuss classical models for a small magnetic particle supporting simplest nonuniform spin distribution, caused by surface anisotropy, which is planar and two-dimensional (2D) model. This means that the spins parallel to one plane and the spin distribution depends effectively on only two space coordinates (x,y). Section II is devoted to the planar continuum 2D model in the limit case of the infinite surface anisotropy, where exact solutions are found and analyzed. In Sec. III the same model will be considered for the case of finite anisotropy. Section IV contains results of direct numerical simulations for the 2D lattice models and the consideration of pinning effects that can be estimated from the continuum model. The analysis of thermal and topological stability is also done in this section. The last section, Sec. V, contains the summary of obtained results and a short discussion of those in with other similar systems.

I. MODEL

There are two approaches to the analysis of the static and dynamic properties of magnetic materials: discrete microscopic and macroscopic. The microscopic approach is based on a discrete spin Hamiltonian in which the spins $\boldsymbol{S}_i$ (quantum or treated quasiclassically, as will be done below) are specified at the lattice sites i. In discrete models the magnetic anisotropy can be introduced in two different ways: as single-ion anisotropy and as anisotropy of the exchange interaction. To describe them, the spin Hamiltonian is chosen in the form

$$\mathcal{H}=\sum_{\langle ij\rangle} J_\alpha S_i^\alpha S_j^\alpha+\sum_i K_\alpha (S_i^\alpha)^2+\sum_i B_{\alpha\beta}(i) S_i^\alpha S_i^\beta. \quad (1)$$

Here S_i^α is the projection of a classical spin on the symmetry axis α of the bulk crystal. The summation in the first term is over all the nearest neighbors in the lattice, J_α is an anisotropic exchange tensor. The constant K_α and function $B_{\alpha\beta}(i)$ describe the volume and the surface single-ion anisotropy energies, respectively. For the crystals with rhombic or higher symmetry, all tensors describing volume characteristics can be diagonalized simultaneously. The tensor function $B_{\alpha\beta}(i)$ is nonzero only near the surface and abruptly decreases in the depth of the sample. The surface creates another chosen direction, a normal to it, and enters a local system of coordinates, in which the tensor $B_{\alpha\beta}(i)$ is diagonal. We neglect in Hamiltonian (1) a dipole-dipole coupling and a Zeeman interaction with an external magnetic field.

We shall use a simple version of Eq. (1) with an uniaxial symmetry for the bulk properties (z as a chosen axis, for definiteness) and with nearest-neighbor interaction only:

$$\mathcal{H}=-J\sum_{i,\delta} (S_i^x S_{i+\delta}^x+S_i^y S_{i+\delta}^y+\lambda S_i^z S_{i+\delta}^z) +K_z\sum_i (S_i^z)^2+B\sum_{i'} (\boldsymbol{S}_{i'}\boldsymbol{n})^2. \quad (2)$$

Here J is the exchange integral, λ is the anisotropy parameter of the exchange interaction, and $\boldsymbol{\delta}$ are the vectors of the nearest neighbors, the summation over i' in the last term includes only the surface sites, where the number of the nearest neighbors differs from the volume one. In order to more adequately compare the lattice and continuum models, we assume that the vector $\boldsymbol{n}$ is a normal to the surface, but not a direction given by the Miller indices.

The sign of the exchange integral plays no role for the statics of nonfrustrated magnets with a bipartite lattice. Moreover, a model without dipole-dipole coupling is more adequate for antiferromagnets than ferromagnets. For simplicity, we use below the ferromagnetic representation of spin distributions, i.e., $J>0$. The transition to the antiferromagnetic case for a bipartite lattice is trivial: we introduce sublattices and change the directions of the spins in one of them.

The continuum approximation of Eq. (1) is based on a free-energy functional $\mathcal{W}[\boldsymbol{m}]$ that depends on the local normalized magnetization $\boldsymbol{m}(\boldsymbol{r})$, $\boldsymbol{m}^2=1$. Using the standard smoothing procedure of a lattice model, we write down the functional $\mathcal{W}[\boldsymbol{m}]$ as

$$\mathcal{W}[\boldsymbol{m}]=\frac{1}{2}\int_\Omega \frac{Sd\boldsymbol{r}}{a^3}\{Ja^2[(\boldsymbol{\nabla} m_x)^2+(\boldsymbol{\nabla} m_y)^2+\lambda(\boldsymbol{\nabla} m_z)^2] +Km_z^2+aB(\boldsymbol{mn})^2\delta(\boldsymbol{r}-\boldsymbol{r}_s)\}. \quad (3)$$

Here Ω is the volume of the particle, the vector $\boldsymbol{r}_s$ parametrizes the surface, $\delta(\boldsymbol{r})$ is the Dirac δ function, a is the lattice spacing, and S is the cross-section area. The solution of the Euler-Lagrange equation for Eq. (3) gives spin configurations with a preferential direction close to the surface. It is clear that the measure of inhomogeneity depends on the problem parameters and the sample shape. A simple consideration shows that for the fixed shape there are only two relevant parameters. The first one is the characteristic radius R/r_0, where $r_0=a\sqrt{J/K}$ at $\lambda=1$ or $r_0=2a\sqrt{\lambda/(1-\lambda)}$ at $K=0$ is the magnetic length, defined in the same way as for bulk materials.[31] The second parameter is the ratio of the exchange integral to the surface anisotropy B/J. To simplify analysis we consider a model with a purely planar spin distribution. Such distributions appear for magnetic vortices at strong enough easy-axis anisotropy, $\lambda<\lambda_c$, where $\lambda_c\sim 0.7$ when $r_0\simeq a$.[32] In this case we obtain the one-parameter model characterized by the ratio B/J. As we will see below, such a model demonstrates a wide set of inhomogeneous states and allows complete analytical and numerical investigations. We restrict ourselves to the case of one more simplification, namely, a model which allows 2D spatial spin distributions, i.e., such distributions which depend only on two spatial variables, say, x and y. Apparently, such a simplification is applicable to an island of a magnetic monoatomic layer shaped as a disk. For numerical simulation we will choose a fragment of the two-dimensional square lattice in the form of a disk. However, applicability of the obtained results is not limited by this concrete case. It is easy to imagine situations where the same spatial-two-dimensional distribution is realized. As an example one can regard a ferromagnetic particle with the volume easy-plane anisotropy, having a form of a cylinder with the base parallel to the easy plane (the x-y plane) and with the axis along the z axis. If one considers that the surface anisotropy constant B in Eq. (3) is positive, then the normal to the surface is the hard axis of the surface anisotropy. It is clear that any planar spin distribution with $S_z(i)=0$ ensures both the minimum of the volume and the surface anisotropy on the upper and bottom cylinder surfaces. In this case nonuniformity is caused only by the lateral cylinder surface, and one can expect that the distribution will be a spatial-two-dimensional one, with the same character as for the purely two-dimensional problem.

II. A STRONG BORDER ANISOTROPY IN A CONTINUUM APPROACH

We shall start from the simplest model to describe effects of surface anisotropy. Consider a disk-shaped (or cylinder-shaped, see above) magnet, with x-y plane as an easy plane, and assume a 2D spin distribution. We assume that the magnetization is a two-dimensional unit vector, in a polar mapping: $m_z=0$ and $\boldsymbol{m}_\perp=\hat{\boldsymbol{e}}_x\cos\phi+\hat{\boldsymbol{e}}_y\sin\phi$, where $(\hat{\boldsymbol{e}}_x,\hat{\boldsymbol{e}}_y,\hat{\boldsymbol{e}}_z)$ is the basis in the spin space and $\phi=\phi(x,y)$ is the angle between $\boldsymbol{m}$ and $\hat{\boldsymbol{e}}_x$. The magnetic energy of the disk takes the form

$$\mathcal{W}[\phi]=JS^2\left[\frac{1}{2}\int_\Omega dS(\boldsymbol{\nabla}\phi)^2+b\int_\Gamma d\chi\cos^2(\phi-\chi)\right]. \quad (4)$$

Here Ω is the area of our disk-shaped magnet with the radius R, the contour Γ is the border circle, and (ρ,χ) are the polar coordinates in the plane of magnet. The parameter b is proportional to the constant of a border anisotropy, $b=(B/J)\times(R/a)$. We choose $b\geqslant 0$, and the preferential surface directions are tangent. This choice is motivated above; one more reason is that such an effective term can be used to model the magnetic dipole interaction.[33] The function $\phi(\rho,\chi)$ may have singularities inside the disk Ω. Minimal configurations for the energy (4) are constructed from solution of the respective Euler-Lagrange equations, which is the scalar Laplace equation

$$\boldsymbol{\nabla}^2\phi=0, \quad (5)$$

with the boundary condition at $\rho=R$,

$$R\frac{\partial\phi}{\partial\rho}\bigg|_{\rho=R}-b\sin 2[\phi(\rho,\chi)-\chi]=0. \quad (6)$$

Thus, this is a problem with a nonlinear boundary condition.

In the absence of the boundary anisotropy, $b=0$, homogeneous solutions $\phi=\text{const}$ satisfy simultaneously Eqs. (5) and (6), and this trivial case is not considered. First of all, we analyze possible solutions in the limit of strong border anisotropy, $b=\infty$, when the problem becomes linear and can be solved exactly. The boundary condition leads to two possible solutions $\phi(R,\chi)=\chi\pm\pi/2$. Such ambiguity of the boundary conditions here differs from the classic internal Neumann problem of mathematical physics and the relevant physics will be discussed below. The solutions in both cases can be constructed via harmonic functions, it can as well be done in two-dimensional electrostatics.[34] The general solution of the Laplace equation ϕ can be written via a complex potential $u(z)$ of integer charges q_k placed at the points z_k:

$$\phi=\text{Im}[u(z)], \quad u(z)=\sum_k q_k\ln(z-z_k)+\text{const}. \quad (7)$$

These charges have a simple physical meaning, they describe well-known in-plane vortices, which have been repeatedly discussed in regard to 2D magnetism. We introduce a complex representation for the coordinate plane xy, $z=x+iy$. The functional $\mathcal{W}[u]$ is rewritten as

$$\mathcal{W}[u]=JS^2\left[\frac{1}{2}\int_0^R\rho d\rho\int_{|z|=\rho}\frac{dz}{iz}\left|\frac{du}{dz}\right|^2 + \frac{b}{8}\int_{|z|=R}\frac{dz}{iz}\frac{(\xi^2-1)^2}{\xi^2}\right], \quad (8)$$

where

$$\xi^2=\frac{z^*}{z}\exp(u-u^*). \quad (9)$$

In the continuum approximation the energy $\mathcal{W}[u]$ is logarithmically divergent, close to points where the in-plane vortices (charges) q_k are placed. To describe these singular solutions in the continuum model, we have to introduce a cutoff parameter of the order of the lattice spacing. Singularities cost much energy, and one could expect that configurations with a global minimum of $\mathcal{W}[u]$ should be sought among the nonsingular functions $u(z)$ in the area Ω or functions with a small number of singularities.

A. Vortexlike configurations

The simplest solution with one singularity is a centered vortex, see Fig. 1, generated by the functions $u=\ln z\pm i\pi/2$ with the energy

$$E_v=JS^2\pi\ln\left(\frac{R}{r_\epsilon}\right), \quad (10)$$

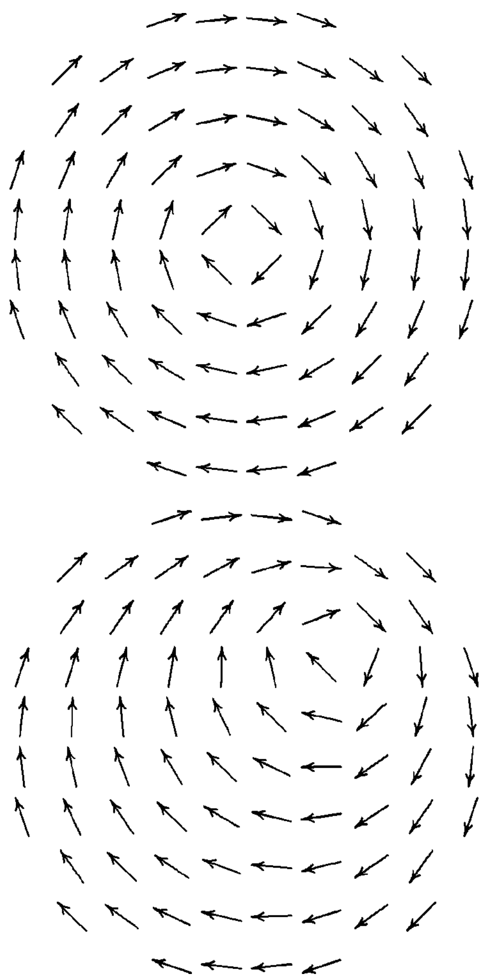

FIG. 1. Numerically calculated vortexlike states for the discrete model (2) with $\lambda=0$, $K_z=0$ and $R=5a$.

where r_ϵ is a cutoff parameter for vortex states of the order of the lattice spacing a. Besides these solutions the others are noncentered vortices for infinite b, see Fig. 1, generated by

$$u(z)=\ln(z-z_0)+\ln\left(z-\frac{R^2}{z_0^*}\right)\pm i\frac{\pi}{2},\quad \text{where } |z_0|\leqslant R, \tag{11}$$

with the vortex placed at the point z_0. They also satisfy the conditions $\phi=\chi\pm\pi/2$ on the border Γ. As seen from Eq. (11), the interaction between the vortex and the border, which may be considered as a consequence of the boundary condition (6), is equivalent to the coupling between the vortex and the image vortex placed outside the disk at the inverse symmetric point with respect to the border circle. The calculation of the energy covers only the area Ω and the singularity of the reflected charge gives no effect. The energy of noncentered vortex for infinite b (fixed boundary conditions $\phi=\chi\pm\pi/2$ on the border) is given by

$$E_v^{(\mathrm{d})}=JS^2\pi\left[\ln\left(\frac{R}{r_\epsilon}\right)-\ln\left(1-\frac{|z_0|^2}{R^2}\right)\right]. \tag{12}$$

The first term coincides to a proper energy of the vortex given by Eq. (10), and the second term is the energy of the interaction between the vortex and the border; it is a repulsive one. Besides it another force acts on the vortex: the vortex tends to escape from a finite area in order to decrease $|\nabla m|$, and thereby being attracted to the border. In the case of $b=\infty$ the repulsive force prevails, the vortex is stabilized at the farthest point from the border, and the second term in Eq. (12) is absent.

B. Configurations with two half vortices on the border

The above considered vortexlike distributions are some of the simplest spin distributions, minimizing surface anisotropy, not only for the circle shape but also for a border in the form of any simple contour. Indeed, going around a simple closed contour, the normal $\boldsymbol{n}$ to it turns to 360°. This means that the topological characteristic of the planar unit vector, so-called *vorticity*,[31] q equals to ±1 for the vector $\boldsymbol{n}$. Obviously, those magnetic vortices having the vorticity $q=1$ are quite probable candidates to realize the energy minimum. Nevertheless, vortices with any $q\neq 0$ admittedly possess singularities inside the sample. The analysis of such distributions where magnetization has no singularities in the bulk is of interest. A simple analysis demonstrates that in this case, as well as for ^{3}He-A, singularities should appear on the border.

To explain this, consider the behavior of the vector field $\boldsymbol{m}=\hat{\boldsymbol{e}}_x\cos\phi+\hat{\boldsymbol{e}}_y\sin\phi$ on the border circle Γ. The boundary condition requires that the vector $\boldsymbol{m}$ be parallel to the border. It can be presented in two ways: $\boldsymbol{m}$ may be parallel or antiparallel to the tangent vector $\hat{\boldsymbol{\tau}}=\boldsymbol{n}\times\hat{\boldsymbol{e}}_z$. Assuming that $\boldsymbol{m}$ is nonsingular inside Ω, the circle Γ can be divided into an even number of alternating regions: in half of them $\boldsymbol{m}$ has to rotate clockwise and in the others counterclockwise. Thus, besides the above considered vortexlike solutions, there exist regular configurations inside the circle Ω and with singularities on the border, see Fig. 2(c). (Such singularities in the three-dimensional case are referred to[30] as vortex lines.) The simplest two-singularity solutions can be written as

$$u(z)=\ln(z-Re^{i\phi_1})+\ln(z-Re^{i\phi_2})+i\pi\pm i\frac{\pi}{2}. \tag{13}$$

This is a field created by two charges placed at the border points $Re^{i\phi_1}$ and $Re^{i\phi_2}$. It is easy to check that the conditions $\phi=\chi\pm\pi/2$ are satisfied on the border wherever $\phi(R,\chi)$ is defined. To calculate the energy thoroughly, we have to introduce the cutoff parameter r'_ϵ and integrate over the disk Ω except two half circles of radius r'_ϵ centered at the charges. Under the condition that the cutoff regions do not overlap, $R(\phi_1-\phi_2)\gg a$, the energy of the configurations are

$$E_{\mathrm{hv}}=JS^2\pi\left[\ln\left(\frac{R}{r'_\epsilon}\right)-\ln 2-\ln\left|\sin\frac{\phi_1-\phi_2}{2}\right|\right]. \tag{14}$$

Here r'_ϵ is the corresponding cutoff parameter. The continuum approximation does not provide a relation between r_ϵ and r'_ϵ and we used numerical calculations for the lattice

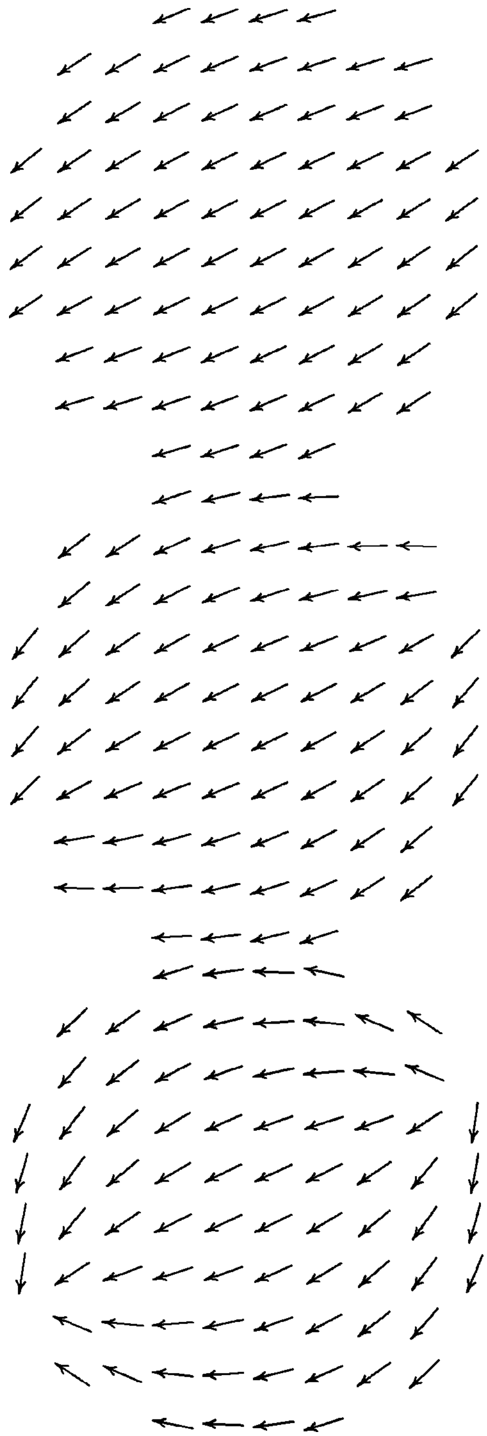

FIG. 2. Minimal nontopological configurations for the discrete model (2) with $\lambda=0$, $K_z=0$, and $R=5a$ for different values of border anisotropy.

model to find it out. These calculations show with a good accuracy that $r_\epsilon = r'_\epsilon$, and we will assume that in the following. The minimum of Eq. (14) is achieved for charges placed at the opposite points of the border, it is given by

$$E_{\rm hv}^{\rm min} = JS^2\pi\left[\ln\left(\frac{R}{r_\epsilon}\right) - \ln 2\right]. \tag{15}$$

Thus, the interaction of surface charges with each other is also repulsive. Comparing the expressions (10) and (15), we see that the energies for both configurations are logarithmically diverged and differing by the constant. Thus, the configuration with two half vortices at the opposite points of the border is preferable to the single vortex for XY model.

III. FINITE VALUES OF A SURFACE ANISOTROPY

In this section we consider the case of a finite surface anisotropy. At $b<\infty$, the boundary condition (6) is nonlinear. It is easy to see that the only centered vortex from all configurations with the vortex inside the sample is an exact solution for any finite values b. A noncentered vortex is not a solution to our problem at finite $b<\infty$. Such states are absent in the continuum model, but they become metastable in the discrete model because of lattice pinning. The numerical calculations show that their energies depend weakly on the surface anisotropy constant. This class will be considered in Sec. IV.

The solutions with two half vortices on the border (13) for finite anisotropy $b<\infty$ transform to nonsingular solutions with two vortices placed *outside* the disk at the opposite points z_0 and $-z_0$, where $|z_0|>R$. This distribution is generated by the function

$$u(z) = \ln(z-z_0) + \ln(z+z_0) + i\pi \pm i\pi/2. \tag{16}$$

The particular exact solutions of problems (5) and (6) with an arbitrary b have been found by Burylov and Raikher[35] for a distribution of the vector director near the surface of a cylindrical solid particle embedded in a monodomain nematic liquid crystal. Using of the boundary condition (6) for the function (16) gives the value of z_0 in the form

$$|z_0|^2 = R^2(1+\sqrt{1+b^2})/b. \tag{17}$$

For such values z_0, the boundary condition (6) satisfy exactly. The energy of the configuration is equal to

$$E_{\rm hv}(b) = JS^2\pi\left[\ln\frac{1+\sqrt{1+b^2}}{2} + b - \frac{b^2}{1+\sqrt{1+b^2}}\right] - 2JS^2\int_0^{\phi_0} x\tan x\,dx. \tag{18}$$

The latter term arises due to the cutoff close to the half vortices which are introduced for $|z_0|-R\leqslant r_\epsilon$, and $\phi_0 = \arccos[(|z_0|-R)/r_\epsilon]$. Its contribution is important for a high enough surface anisotropy, $B\gtrsim J$ only, see Fig. 2(c).

It is easy to see that for any finite b the energy of the two-charge configuration is lower than its limit value (15), and it decreases monotonically with decreasing b. Another limit case of small surface anisotropy $b\to 0$ leads to the almost homogeneous distribution $\boldsymbol{m}$, see Fig. 2(a), with the nearly zero energy $E=JS^2\pi b$. When b increases, the vector field $\boldsymbol{m}$ is curved to the diametrically pair of points, and the energy increases, see Fig. 2(c). These features are in good agreement with that obtained numerically for discrete finite system. The dependency of $E_{\rm hv}$ versus the surface anisotropy

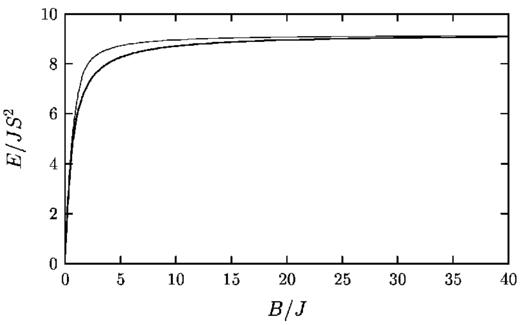

FIG. 3. The dependence of the energy of the minimal configuration vs the surface anisotropy for the disk with the radius $R=10a$. The thin line is a two-charge approximation; the thick line is a numerically calculated result for the lattice model.

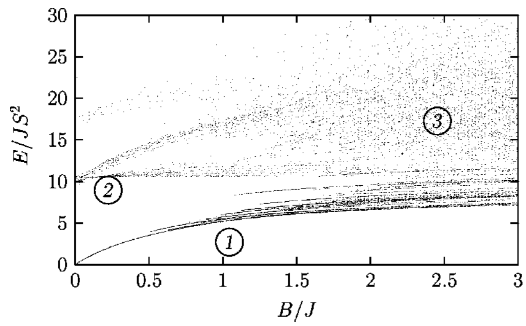

FIG. 4. Metastable configurations for the $R=8a$ disk. Shown are approximately 3×10^4 dots. Regions "1" and "2" are shown in Figs. 5 and 6.

B from Hamiltonian (2) is plotted in Fig. 3 together with that for continuum model (4). The discrepancy of the curves is connected with the discreteness effects, which are important for small samples, for larger system radius (the value of R till $R=30a$ has been used). In the case of $b\rightarrow\infty$ the vortex energy is higher than the two-charge configuration energy for XY model, and the vortex states are also metastable for any finite b.

IV. NUMERIC SIMULATION AND LATTICE EFFECTS

For our model with rather strong volume and surface anisotropy, the characteristic size is $|\nabla m|\sim a^{-1}$, and it is not obvious that effects of discreteness can be neglected. An exact analysis of the discrete model requires numerical calculations, but some qualitative results can be obtained using the lattice potential method. For a direct numerical simulation we basically used the XY model with $\lambda=0$, i.e., with an extremely strong easy-plane anisotropy (some results concerning the finite λ will be discussed in Sec. V).

A. Numerical simulation

For numerical calculation of the equilibrium states we started from the discrete Hamiltonian for the magnetic energy (2). Calculations have been performed starting from a random initial configuration or from a configuration given by Eq. (7) with constants z_k, q appropriate for a considered problem. The energy minimization has been performed through a Seidel-like algorithm with the successive exact solution of the local equilibrium equation for a fixed site that can be obtained from the following one-site energy:

$$E_L=-\boldsymbol{S}\boldsymbol{H}+\frac{B}{2}(\boldsymbol{S}\boldsymbol{n})^2-\frac{\mu}{2}\boldsymbol{S}^2, \qquad (19)$$

where μ is a Lagrange multiplier for the condition $|\boldsymbol{S}|=1$ and $\boldsymbol{H}=J\Sigma_{\langle\rangle}(S^x\hat{\boldsymbol{e}}_x+S^y\hat{\boldsymbol{e}}_y+\lambda S^z\hat{\boldsymbol{e}}_z)$ is the effective field created by the nearest neighbors of the fixed site. The term with B is present for the border spins only. In a simple case $B=0$ we obtain $\boldsymbol{S}=\boldsymbol{H}/|\boldsymbol{H}|$. When $B\neq0$ a more complicated analysis of the roots of the equilibrium condition $dE_L/d\boldsymbol{S}=0$ is needed. Among these roots $\boldsymbol{S}_{\min}$, we choose the value that gives the deepest minimum of E_L. For all minimizations we observe that this procedure converges to one of the stable configurations. The configuration appearing during minimization energy process was mainly dictated by the choice of the initial configuration.

In order to explore all metastable minimal configurations in the lattice model (2) with $\lambda=0$, we performed more than 10^7 minimization procedures in accordance with the described scheme. Initial configurations and the surface anisotropy B are chosen randomly. The obtained energy values are presented by dots on the plane $(B/J,E/JS^2)$, see Fig. 4, the system size is chosen small enough to show a discrete nature of the possible states. Such an analysis allows to judge both the energy absolute minimum for a given B/J and the presence of metastable states. It is seen that in some plane regions (marked as "1" and "2") the dots are grouped in more or less well-defined lines, which obviously correspond to the most stable states and describe the dependence of their energies on b. The characteristic regions are present in Figs. 5 and 6. The region (marked as "3"), in which the dots are distributed practically randomly (in fact, there the dots are also fitted by lines), corresponds to high-energy states. They are not subjects of interest. To classify the spin states the positions of singularities of the function $\phi(x,y)$ have been analyzed numerically and the positions of poles (vortices), which are placed inside of a disk or on its border, have been obtained. Such an analysis demonstrated the presence of all states described above, including noncentered vortices and states with nonsymmetrically placed surface singularities, but yet some less favorable states, namely, antivortices with the distribution like $\phi=-\chi+\text{const}$, where χ is the polar

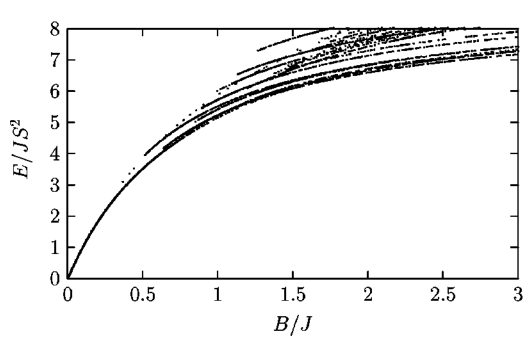

FIG. 5. Minima with two half vortices for the $R=8a$ disk.

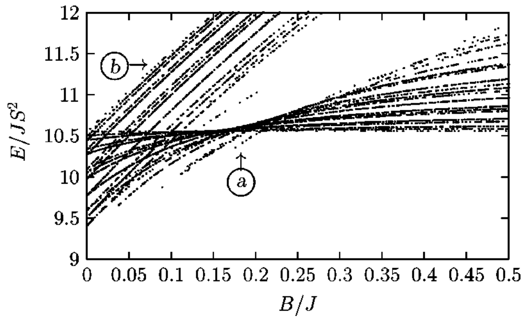

FIG. 6. Vortex minima close to $B=0$ for the $R=8a$ disk.

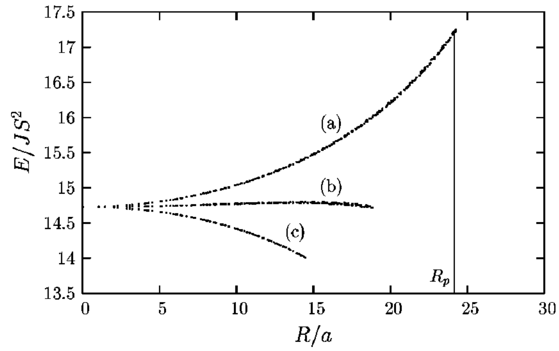

FIG. 7. The energy of a noncentered vortex vs its displacement for three values of surface anisotropy: (a) $B/J=0.4 \gg B_c$ (attraction to the center), (b) $B/J=0.04 \simeq B_c$ (equilibrium), and (c) $B/J=0.004 \ll B_c$ (repulsion from the center). Radius of the disk is $30a$. The radius of the pinning region ($R_p \sim 24$) is maximal for the largest value of B and decreases for lower values.

coordinate, instead of $\phi=\chi+\text{const}$, characteristic of vortices. Let us discuss the obtained results.

First of all, the given analysis has confirmed that the symmetrical states with two singularities possess the minimal energy. In the region of the small anisotropy and energy $E \lesssim 4.0$ (here and after energy values are presented in units of JS^2) only state with symmetric half vortices are present, see details of this region in Fig. 5. At $B/J \gtrsim 0.5$ other well-defined lines of dots appear, which also correspond to states with two half vortices, however, with broken symmetry. These states have higher energy and they are unstable at small B, but at larger B they become metastable due to surface pinning effects. With increasing B the pinned states appear in the vicinity of nonregular regions of a surface, which result from cutting out a disk from the square lattice. With further increase of $B/J \geqslant 1.5$–2, the number of asymmetric states grows.

The second interesting region of plane at the energy $E \sim 10$ corresponds to vortex states. Its details at small B/J are depicted in Fig. 6. It is worth noting that according to the analytical consideration the centered vortex presents at any B and its energy does not depend on B. Besides that state there exist noncentered vortices stabilized by the lattice pinning. Since the state with noncentered vortex at finite b is not an exact solution (unlike the nonsingular case), they will be analyzed numerically in the following subsection with a simple qualitative model of pinning. At large enough anisotropy the energies of noncentered vortices are higher compared to the state with the centered vortex. However, at small anisotropy ($B/J \leqslant 0.2$ for the system size $R=8a$ used for Figs. 4–6) an interesting effect emerges: noncentered vortices become more favorable than the centered one (the correspondent region marked as "a"). This effect could be described as a change of the sign of the effective interaction between the vortex and the border at some value $B=B_c$. (Let us remind that the case $B=\infty$ corresponds to fixed boundary conditions, while the case $B=0$ corresponds to free boundary conditions, which are associated with repulsion and attraction of the vortex to the border, respectively, see Ref. 31.) This effect is present also for big values of the radius, see Fig. 7, in which is plotted the vortex energy calculated in model (2) versus its displacement for three values of surface anisotropy and the radius $R=32a$. The characteristic value of the surface anisotropy B_c decreases inversely proportional to the system size. The values found numerically for $R=(5$–$30)a$ can be extrapolated by the dependence $B_c/J \sim 1.2(a/R)$.

At $B=0$ the vortex and antivortex have the same energy and in the region of extremely small B antivortices are also reliably observable, see Fig. 6, region "b." However, when B increases, the energy of antivortices grows rapidly and we do not discuss them.

B. Lattice effects and vortex stability

For nonuniform states the lattice pinning of singular points in the spin distribution both vortices and surface singularities (half vortices) play an essential role. It is interesting to discuss such points in more details. The continuum model neglects a discrete nature of crystals and the pinning effects. The simplest way to describe analytically lattice effects and, in particular, to investigate the local stability of metastable states, is to introduce an effective periodical potential (Peierls-Nabarro potential) into the continuum model. Schnitzer shows,[36] see also Ref. 31, that for in-plane vortices this potential is independent of the values of out-of-plane anisotropy parameters (for $\lambda < 0.8$) and can be presented in the simplest form as $U_{PN}(x,y)=\kappa JS^2 \pi[\sin^2(x\pi/a)+\sin^2(y\pi/a)]$, where the origin is chosen at the point which is equidistant from lattice sites, and the numeric parameter $\kappa \simeq 0.200$.[36] The potential minima are attained at all points like $\boldsymbol{r}=n\boldsymbol{e}_x+m\boldsymbol{e}_y$, where m, n are integers, $|\boldsymbol{e}_x|=|\boldsymbol{e}_y|=a$, and the saddle points are at $(n+1/2)\boldsymbol{e}_x+m\boldsymbol{e}_y$ and $n\boldsymbol{e}_x+(m+1/2)\boldsymbol{e}_y$. A metastable state with a vortex shifted from the center to the point $\boldsymbol{r}$ exists only when the sum $E(\boldsymbol{r})=E_v(\boldsymbol{r},b)+U_{PN}(\boldsymbol{r})$ has a minimum at this point. The loss of stability manifests itself as ruptures of lines in Figs. 5 and 6, see also Fig. 7.

Then it is easy to show that the noncentered vortices are held by the pinning potential and are stable if their coordinates are inside the circle of radius R_p. The radius of the pinning region R_p is determined from the explicit expression (12) for the energy of the vortex placed at the point r_0 as

$$a\frac{dE^{(\mathrm{d})}_{\mathrm{vor}}(r_0)}{dr_0}\bigg|_{r_0=R_p}=\frac{\pi\kappa}{a}, \tag{20}$$

and the case $a \ll R$ leads to $R_p = R - a/\kappa$.

Thus the vortices can be pinned everywhere inside the sample except the thin strip close to the border. Their energies relative to the zero level of the centered vortex lie in the band of the width $\sim J\ln(R/a)$. Such states are frequently observed in numeric simulations for the discrete model when initial configurations for the minimization are chosen randomly.

Although a detailed analysis of thermal fluctuations and decay of metastable states is beyond the scope of this work, their role can be discussed on the basis of the previous estimates. The above introduced R_p is the radius of the region where pinning disappears, i.e., at $r \to R_p$ the barrier height separating states with a vortex placed in adjacent lattice sites, becomes to zero. It is also reasonable to introduce the function $R_p(E)$, such that at $r < R_p(E)$ the barrier height between these two states is higher than some value E. Naturally, $R_p(E) \to R_p$ at $E \to 0$, $R_p(E) \to 0$ at $E \to E_b^{\max}$, where $E_b^{\max} = \kappa J S^2 \pi$ is the maximal pinning energy. For intermediate region $E \ll E_b^{\max}$, a simple calculation yields

$$-R_p(E)=\frac{a}{\kappa}\,\frac{E_b^{\max}}{E_b^{\max}-E}, \tag{21}$$

and for all values of $E_b^{\max} - E \sim E_b^{\max}$ the value of $R_p(E)$ is again near R. Thus, the role of thermal fluctuations at $k_B T \ll E_b^{\max}$ can be considered as negligently small, and the above described metastable states may be manifest as long-lived ones even for finite temperature. On the other hand at $k_B T \geq E_b^{\max}$ metastable states such as the noncentered vortex will not be manifest and only the centered vortex should be considered.

For two-charge configurations the lattice potential also creates other metastable configurations with higher energies than the energy of configurations with maximally separated charges. Their analysis is similar to the one that has been performed for the case of a noncentered vortex. Two pinned charges on the border can be approached only down to the angle $\phi_p = |\phi_1 - \phi_2| \simeq \pi a/\kappa R$. Consideration of thermal fluctuations can be done for noncentered vortices as well and it leads to the similar results, practically all such states are metastable.

In conclusion of this section we discuss the stability of vortices as a topologically nontrivial configuration under transformation to nontopological one. Inside of two topologically different classes of states—with vortex or with two surface singularities—effective relaxation to the most favorable state inside the given class is possible. However, the previous results show that the vortexlike configurations with the centered vortex have higher energy than the two-charge configuration, and are metastable. Therefore, the state with centered vortex may relax toward the most profitable state with two surface singularities. The simplest scenario of the vortex decay is the following. The vortex moves to the nearest point on the border and its counterpart also moves to it. The point, where they merge, is a saddle point of the path with the energy $E_{\mathrm{sad}} = JS^2\pi\ln(R/\epsilon)$ over the centered vortex energy. This state is referred as a *boojum* or *fountain* in the ^{3}He theory,[30,37] where it is a true minimum. Further, the merged charges decouple and move along the border: one—in the clockwise direction and another—in the counterclockwise direction to the most distant positions. Thus, the energy E_{sad} is the barrier height between the two classes of configurations, and it can be used for the analysis of a thermal (or quantum tunneling, for low temperature) decay of vortex states. Note that the barrier is nothing to do with the pinning potential. Its value does not contain the parameter κ, but it is proportional to $\ln(R/a)$ and is much higher than the exchange energy JS^2. Thus, vortex states can be stable even at high enough temperature comparing with the Curie temperature $T_c \sim JS^2$, and the probability of the decay of the vortex state is very low even at the temperatures comparable with T_c.

V. CONCLUDING REMARKS

A strong surface anisotropy for easy-plane Heisenberg magnets destructs the homogeneous ordering and leads to the two types of static structures: the vortex state and the state with pair of half vortices on the surface. For finite anisotropy the latter state becomes nonsingular. This state is energetically favorable for all finite values of surface anisotropy. The energy gap between it and the vortex state is of the order of the exchange energy, but the energy barrier is much higher than the exchange energy. The strong bulk anisotropy leads to well-pronounced effects of lattice pinning, and large number of metastable states appears as well.

It is interesting to compare these results to those which have been obtained for fine particles made with soft magnetic materials such as permalloy magnetic dots, where the nonuniform states are caused by the magnetic dipole interaction. The common point for these cases is not only the presence of the vortex state but also the presence of nontopological nonuniform states, leaf or flower states.[6,10–12] The distinction consists in the fact that for soft magnetic particles there are nonsingular vortices with the out-of-plane magnetization component while in our problem with the strong bulk anisotropy the only in-plane vortices with a singularity are present. It is likely that in virtue of this for permalloy particles there is a very much pronounced transition from the vortex state to the nontopological one with the system size decreasing, while in our problem the vortex state is always less favorable energetically. It is worth noting that our preliminary numerical data indicate the appearance of such a transition at a weak easy-plane anisotropy; an extended discussion of this problem is beyond the scope of the present work.

It is also interesting to note that the spin distribution in the nonsingular state of our 2D problem resembles the distribution having axial symmetry and the plane of symmetry perpendicular to the axis obtained by Dimitrov and Wysin[21,22] for 3D particles where both the volume and surface anisotropies are presented. Recently, the stable three-dimensional analog of vortices, hedgehog configuration has been discovered for a ball-shaped particle with strong normal border anisotropy by numeric calculations.[38] On the other hand, for the superfluid ^{3}He-A, which is defined in terms of our model by use of the infinitely strong surface anisotropy and isotropic volume properties, the true minimum constitutes less symmetric state (boojum or fountain) with one surface singularity and without the symmetry plane.[30,37] In our case the boojumlike distribution appears only for nonstable saddle point, which separates the vortex and nonsingular states.

The authors thank C. E. Zaspel, A. Yu. Galkin, and A. K. Kolezhuk for fruitful discussions and help. This work was supported by the INTAS, Grant No. 97-31311 and partially by Volkswagen Stiftung, Grant No. I/75895. One of us (B.I.) thanks the Montana State University for kind hospitality (NFS Grants No. DMR-9974273 and No. DMR-9972507).

*Electronic address: kireev@imag.kiev.ua
†Electronic address: bivanov@i.com.ua

[1] S.O. Demokritov, B. Hillebrands, and A.N. Slavin, Phys. Rep. **348**, 441 (2001).
[2] B. Hillebrands, C. Mathieu, C. Hartmann, M. Bauer, O. Büttner, S. Riedling, B. Roos, S.O. Demokritov, B. Bartenlian, C. Chappert, D. Decanini, F. Rousseaux, E. Cambril, A. Müller, B. Hoffmann, and U. Hartmann, J. Magn. Magn. Mater. **175**, 10 (1997).
[3] E.F. Wassermann, M. Thielen, S. Kirsch, A. Pollmann, H. Weinforth, and A. Carl, J. Appl. Phys. **83**, 1753 (1998).
[4] R.P. Cowburn, D.K. Koltsov, A.O. Adeyeye, M.E. Welland, and D.M. Tricker, Phys. Rev. Lett. **83**, 1042 (1999).
[5] C. Miramond, C. Fermon, F. Rousseaux, D. Decanini, and F. Carcena, J. Magn. Magn. Mater. **165**, 500 (1997).
[6] K. Runge, Y. Nozaki, Y. Otani, H. Mayajima, B. Pannetier, T. Matsuda, and A. Tonomura, J. Appl. Phys. **79**, 5075 (1996).
[7] P.D. Ye, D. Weiss, K. von Klitzing, K. Eberl, and H. Nickel, Appl. Phys. Lett. **67**, 1441 (1995).
[8] S. Sun, C.B. Murrey, D. Weller, L. Folks, and A. Moser, Science **287**, 1989 (2000).
[9] J.F. Smyth, S. Schultz, D.R. Fredkin, D.P. Kern, S.A. Rishton, H. Schmid, M. Cali, and T.R. Koehler, J. Appl. Phys. **69**, 5262 (1991).
[10] N.A. Usov and S.E. Peschany, J. Magn. Magn. Mater. **135**, 111 (1994).
[11] R.P. Cowburn and M.E. Welland, Phys. Rev. B **58**, 9217 (1998).
[12] R.P. Cowburn, A.O. Adeyeye, and M.E. Welland, Phys. Rev. Lett. **81**, 5414 (1998).
[13] N.A. Usov and S.E. Peschany, J. Magn. Magn. Mater. **118**, L290 (1993).
[14] A. Fernandez and C.J. Cerjan, J. Appl. Phys. **87**, 1395 (2000).
[15] T. Pokhil, D. Song, and J. Nowak, J. Appl. Phys. **87**, 6319 (2000).
[16] J. Shi, S. Tehrani, and M.R. Scheinfein, Appl. Phys. Lett. **76**, 2588 (2000).
[17] T. Shinjo, T. Okuno, R. Hassdorf, K. Shigeto, and T. Ono, Science **289**, 930 (2000).
[18] D. Johnson, P. Perera, and M.J. O'Shea, J. Appl. Phys. **79**, 5299 (1996).
[19] M.J. O'Shea and P. Perera, J. Appl. Phys. **76**, 6174 (1994).
[20] M.J. O'Shea and P. Perera, J. Magn. Magn. Mater. **156**, 141 (1996).
[21] D.A. Dimitrov and G.M. Wysin, Phys. Rev. B **50**, 3077 (1994).
[22] D.A. Dimitrov and G.M. Wysin, Phys. Rev. B **51**, 11 947 (1994).
[23] D.A. Garanin and H. Kachkachi, Phys. Rev. Lett. **90**, 065504 (2003).
[24] D.L. Mills, Phys. Rev. Lett. **20**, 18 (1968).
[25] R.W. Wang, D.L. Mills, E.E. Fullerton, J.E. Mattson, and S.D. Bader, Phys. Rev. Lett. **72**, 920 (1994).
[26] B.A. Ivanov, A.Y. Volk, and A.Y. Merkulov, Low Temp. Phys. **28**, 25 (2002).
[27] V.P. Shilov, Y.L. Raikher, J.-C. Bacri, F. Gazeau, and R. Perzynski, Phys. Rev. B **60**, 11 902 (1999).
[28] A. Aharoni, J. Appl. Phys. **61**, 3302 (1987); **69**, 7762 (1991); **81**, 830 (1997); **87**, 5526 (2000).
[29] P.G. de Gennes, *The Physics of Liquid Crystals* (Clarendon Press, Oxford, 1974).
[30] N.D. Mermin, in *Quantum Fluids and Solids*, edited by S.B. Trickey, E.D. Adams, and J.W. Duffey (Plenum Press, NY, 1977), p. 3; P.W. Anderson and R.G. Palmer, *ibid.*, p. 23.
[31] B.A. Ivanov, H.J. Schnitzer, F.G. Mertens, and G.M. Wysin, Phys. Rev. B **58**, 8464 (1998).
[32] G.M. Wysin, Phys. Rev. B **49**, 8780 (1994).
[33] B.A. Ivanov and C.E. Zaspel, Appl. Phys. Lett. **81**, 1261 (2002).
[34] L.D. Landau and E.M. Lifshitz, *Electrodynamics of Continuous Media* (Pergamon Press, NY, 1960).
[35] S.V. Burylov and Y.L. Raikher, Phys. Rev. E **50**, 358 (1994).
[36] H.-J. Schnitzer, Ph.D. thesis, Universität Bayreuth, 1996.
[37] N.D. Mermin, Rev. Mod. Phys. **51**, 591 (1979).
[38] Y. Labaye, O. Crisan, L. Berger, J.M. Greneche, and J.M.D. Coey, J. Appl. Phys. **91**, 8715 (2002).
[39] An alternative explanation based on the hypothesis of the presence of a random single-ion bulk anisotropy have been done by the authors of Refs. 18–20.